

# Excited-State Intramolecular Charge-Transfer Dynamics in 4-Dimethylamino-4'-cyanodiphenylacetylene: An Ultrafast Raman Loss Spectroscopic Perspective

Arvind Barak,<sup>[a]</sup> Nishant Dhiman,<sup>[a]</sup> Floriane Sturm,<sup>[b]</sup> Florian Rauch,<sup>[b]</sup>  
Yapamanu Adithya Lakshmana,<sup>[c]</sup> Karen S. Findlay,<sup>[d]</sup> Andrew Beeby,<sup>[d]</sup> Todd B. Marder,<sup>\*,[b]</sup>  
and Siva Umaphathy<sup>\*,[a, e]</sup>

Photo-initiated intramolecular charge transfer (ICT) processes play a pivotal role in the excited state reaction dynamics in donor-bridge-acceptor systems. The efficacy of such a process can be improved by modifying the extent of  $\pi$ -conjugation, relative orientation/twists of the donor/acceptor entities and polarity of the environment. Herein, 4-dimethylamino-4'-cyano-diphenylacetylene (DACN-DPA), a typical donor- $\pi$ -bridge-acceptor system, was chosen to unravel the role of various internal coordinates that govern the extent of photo-initiated ICT dynamics. Transient absorption (TA) spectra of DACN-DPA

in *n*-hexane exhibit a lifetime of  $> 2$  ns indicating the formation of a triplet state while, in acetonitrile, a short time-constant of  $\sim 2$  ps indicates the formation of charge transferred species. Ultrafast Raman loss spectroscopy (URLS) measurements show distinct temporal and spectral dynamics of Raman bands associated with  $\text{C}\equiv\text{C}$  and  $\text{C}=\text{C}$  stretching vibrations. The appearance of a new band at  $\sim 1492\text{ cm}^{-1}$  in acetonitrile clearly indicates structural modification during the ultrafast ICT process. Furthermore, these observations are supported by TD-DFT computations.

## Introduction

Photoinduced charge transfer is a fundamental step in many chemical and biological processes,<sup>[1,2]</sup> including photosynthesis,<sup>[3]</sup> in which a donor-acceptor pair enables directional electron transfer leading to a long-lived charge-separated state. Photoinduced charge transfer in molecular systems,

particularly in  $\pi$ -conjugated donor-acceptor (DA) systems, is of broad interest from the perspective of organic light-emitting diodes,<sup>[4]</sup> organic semiconductor devices,<sup>[5–7]</sup> fluorescent molecular sensors,<sup>[8]</sup> and in the development of materials with large second-order nonlinearities<sup>[9]</sup> due to the presence of low lying charge transfer states. Upon photoexcitation of such molecules, an intramolecular charge transfer (ICT) between the donor and acceptor entities leads to a polar state.<sup>[10]</sup>

Upon photoexcitation, *N,N*-dimethylaminobenzonitrile (DMABN), exhibits an ICT process from the *N,N*-dimethylamino group to the cyano group.<sup>[11–13]</sup> Extensive research has been carried out to understand the intricacies involved in the excited state dynamics of DMABN.<sup>[14–16]</sup> DMABN, in polar solvents, exhibits a dual band fluorescence, in which the shorter wavelength emission is due to a locally excited (LE) state and the longer wavelength emission arises from the charge transfer state. The charge transfer dynamics from LE to ICT states is accompanied by structural changes and solvent reorganization. The dynamic aspects associated with the charge transfer and structure have been of interest from a theoretical perspective.<sup>[17–20]</sup> The charge transfer process in DMABN is typically described using a model based on twisted intramolecular charge transfer (TICT),<sup>[21]</sup> wherein the dimethylamino group (donor) undergoes a torsional motion while charge is transferred to the benzonitrile moiety (acceptor) leading to a perpendicular TICT state. As a consequence of such a TICT state with a  $90^\circ$  twist of the dimethylamino group with respect to the phenyl ring, electronic decoupling is pronounced between the donor and the acceptor moieties along with a loss of conjugation in the molecule that enables a complete charge transfer between the entities. In the case of a planar ICT (PICT)


[a] A. Barak, N. Dhiman, Prof. Dr. S. Umaphathy  
Department of Inorganic and Physical Chemistry  
Indian Institute of Science  
Bangalore, India-560012  
E-mail: umaphathy@iisc.ac.in


[b] F. Sturm, Dr. F. Rauch, Prof. Dr. T. B. Marder  
Institut für Anorganische Chemie und Institute for Sustainable Chemistry & Catalysis with Boron (ICB)  
Julius-Maximilians-Universität Würzburg  
97074 Würzburg, Germany  
E-mail: todd.marder@uni-wuerzburg.de

[c] Dr. Y. A. Lakshmana  
School of Chemistry  
Indian Institute of Science Education and Research Thiruvananthapuram  
Vithura, Thiruvananthapuram, India-695551

[d] Dr. K. S. Findlay, Prof. Dr. A. Beeby  
Department of Chemistry  
University of Durham  
South Road, Durham DH1 3LE, United Kingdom

[e] Prof. Dr. S. Umaphathy  
Department of Instrumentation and Applied Physics  
Indian Institute of Science  
Bangalore, India-560012

 Supporting information for this article is available on the WWW under <https://doi.org/10.1002/cptc.202200146>

 © 2022 The Authors. ChemPhotoChem published by Wiley-VCH GmbH. This is an open access article under the terms of the Creative Commons Attribution License, which permits use, distribution and reproduction in any medium, provided the original work is properly cited.

model,<sup>[22–24]</sup> the ICT state typically acquires a partially quinoidal planar resonance structure. Over the past few decades, many donor- $\pi$ -bridge-acceptor systems have been examined to address various applications.<sup>[25–31]</sup> However, the efficacy of such a charge transfer process relies on factors related to the nature of donor, acceptor, bridge, and solvent environment.<sup>[32–37]</sup> Extended  $\text{C}\equiv\text{C}$  triple bonded conjugated systems are linear and maintain a high degree of conjugation,<sup>[38]</sup> and have applications in the field of molecular wires and opto-electronics.<sup>[39,40]</sup> A new class of fluorometric and Raman probes for selective sensing of DNA, RNA, and proteins has recently been developed.<sup>[41,42]</sup> Several studies have been reported on the intricacies involved during the ICT process in DA systems particularly associated with extended polyene type bridges.<sup>[43–45]</sup> It was reported that the charge recombination process is directly affected by the type of DA bridge spacer.<sup>[43]</sup> However, studies on ICT in DA systems involving alkynyl bridges are less common. Herein, we analyze the structural dynamics of a D-bridge-A system, 4-dimethylamino-4'-cyanodiphenylacetylene (DACN-DPA), in which the bridge is a diphenylacetylene group. The molecular structure of DACN-DPA is depicted in Figure 1. Excited state properties of diphenylacetylene (DPA) have been reported in detail.<sup>[46–52]</sup> The presence of a donor and acceptor on DPA alters its excited state landscape.<sup>[53,54]</sup>

Earlier steady-state emission studies of DACN-DPA in polar solvents established that an ICT process occurs with a typically large Stokes-shifted emission.<sup>[55]</sup> Hirata and coworkers<sup>[55]</sup> demonstrated, in their picosecond transient absorption and time-resolved emission studies of DACN-DPA, that the excited state lifetime and excited state relaxation pathways are significantly dependent on the solvent polarity. In *n*-hexane (*n*-hex), a non-polar solvent, the LE state decays with a time constant of 650 ps while forming a triplet state. In contrast, in acetonitrile (MeCN), a polar environment, an ICT state forms within an ultrafast timescale which subsequently decays back to the ground state with a lifetime of 0.9 ns. However, the early time dynamics related to the charge transfer process could not be probed due to their experimental limitations. Later, Lim and coworkers<sup>[56]</sup> employed femtosecond time-resolved absorption and emission methods to show that the ICT state in acetonitrile is formed in an ultrashort time scale ( $<1$  ps) from a locally excited state. Such time-resolved absorption and emission methods enable one to resolve the lifetimes of the LE and CT states. However, the intricate structural dynamics of the solute while evolving from the LE to the CT state in different polarity environments could not be extracted from such time-resolved absorption and emission studies. In the present study, we focus on elucidating the early time structural modification in DACN-DPA that eventually governs the excited-state charge transfer dynamics upon photoexcitation.

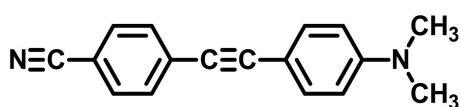


Figure 1. Molecular structure of DACN-DPA.

Lim and coworkers<sup>[57,58]</sup> carried out time-dependent density functional (TD-DFT) and single excitation configuration interaction (CIS) calculations on the DPA system and showed that there exist two close-lying excited  $\pi\pi^*$  and dark  $\pi\sigma^*$  states having a shallow energy barrier. The presence of the electron-withdrawing and electron-donating groups in DACN-DPA can have a significant effect on the energy barrier. Initially, the state switching process in the case of DACN-DPA was proposed to occur from the excited planar  $\pi\pi^*$  state to more polar  $\pi\sigma^*$  state via a *trans*-bent form, and such switching was solvent polarity dependent. Later, Lim and coworkers<sup>[56]</sup> clearly showed the formation of a TICT( $\sigma^*$ ) state, wherein the electron-accepting benzonitrile (BN) group is in a perpendicular orientation to the electron-donating 4-(dimethylamino)-phenylethynyl (DMAB) group and the overall geometry was confirmed to be in the *trans*-bent form.

Furthermore, Amatatsu<sup>[59]</sup> employed *ab initio* complete active space self-consistent field (CASSCF) and its 2<sup>nd</sup>-order multireference Moller-Plesset perturbation (MRMP2) methods to understand the photophysical behavior of DACN-DPA in solution. It was proposed that, in a non-polar solvent, photo-excited DACN-DPA relaxes to the ground state without any twist and has a low probability to pass over the conical intersection between CT and a diradical character state. Hence, DACN-DPA is globally stabilized to a *trans*-bent geometry with a diradical character. However, in polar solvents, electronically excited DACN-DPA with an ICT character can be stabilized by the twist of the dimethylanilino group instead of the less polar *trans*-bent form which assists a charge separation geometrically. However, Harriman and coworkers<sup>[60]</sup> identified a twist around the central alkynylene bond in the case of 4-cyano-(4'-methylthio)diphenylacetylene in water as a polar medium using quantum chemical calculations. In fact, these interpretations are predominantly based on the time-resolved absorption and emission studies and TD-DFT calculations.

Time-resolved infrared (TRIR) experiments have recently been conducted to understand better the dynamics of photo-induced charge transfer in alkyne-linked DA systems.<sup>[61,62]</sup> An allene-alkyne based photoisomerization has been experimentally proposed by Vauthey and coworkers.<sup>[61]</sup> Kubicki and coworkers<sup>[62]</sup> employed an alkyne and a nitro group (electron acceptor) as the vibrational markers to understand better the ultrafast ICT process in D- $\pi$ -A systems with DPA and bis(phenylethynyl)benzene bridges. They also proposed the independence of the  $\pi$ -bridge length on the charge transfer process.

UV-vis transient absorption<sup>[63]</sup> measurements essentially describe the overall time-evolution of the excited state population while the crucial structural modifications that might have significant role in the excited-state charge transfer process are not explicitly visualized. Elucidation of the structural changes during the population dynamics from the initially prepared Franck-Condon (FC) state enables understanding of the transient species that play a crucial role in the subsequent reaction dynamics. DACN-DPA possess various vibrational modes such as  $\text{C}\equiv\text{C}$  stretching, phenyl ring vibrations, etc. Here, we demonstrate how these internal vibrational coordinates/

molecular vibrations in DACN-DPA play a significant role or are influenced during the ICT process. We employ ultrafast Raman loss spectroscopy (URLS)<sup>[64–67]</sup> with high temporal and spectral resolutions to unravel the structural dynamics of the transient species during the ICT process.

## Results and Discussion

### Steady-state absorption, fluorescence and Raman spectra

The steady-state absorption and fluorescence spectra (at 350 nm excitation wavelength) of DACN-DPA in MeCN, dichloromethane (DCM) and *n*-hexane are shown in Figure 2. The computed absorption spectra are shown in Figure S2, and the corresponding oscillator strengths and the major contributions are given in Table S1 in the Supporting Information (SI). As evident from Table S1, excitation at 320 nm has a contribution of 88% from the HOMO to LUMO transition (Figure S1 (a,b)). The associated electron density difference map (EDDM), shown in Figure S1 (c), clearly indicates the formation of an ICT state. The absorption and emission spectra presented herein are consistent with the earlier reports. The absorption maximum of the lowest energy transition is centered at ~365 nm in both solvents, corresponding to the  $S_1 \leftarrow S_0$  ( $\pi\pi^*$ ) transition. However, in non-polar *n*-hexane solvent, the absorption spectrum exhibits a vibronic structure and the fluorescence spectrum shows mirror image symmetry. This is a clear indication of an insignificant interaction between *n*-hexane and DACN-DPA in the excited state.

A very small Stokes shift of ~700  $\text{cm}^{-1}$  clearly indicates that the emitting state is not very polar and lacks ICT character. However, in the polar solvent MeCN, the fluorescence emission is structureless along with a large Stokes shift of 8700  $\text{cm}^{-1}$ . These features clearly indicate that the excited state is significantly stabilized by the polar environment and, as a result, formation of the ICT state is prominent. The emissions of DACN-DPA in *n*-hexane and MeCN arise from a relatively less stabilized ICT state and more stabilized polar ICT state, respectively.

The steady-state Raman spectrum of DACN-DPA in MeCN along with the computed Raman activity are shown in Figure 3. The experimental (in *n*-hexane, solid-state) and theoretical

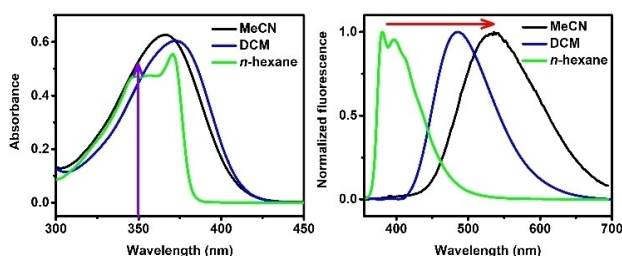


**Figure 2.** (a) UV-vis absorption and (b) fluorescence spectra at 350 nm of DACN-DPA in MeCN (black), DCM (blue) and *n*-hexane (green). The violet and red arrows represent the excitation wavelength and the Stokes shift of the emission spectrum, respectively.

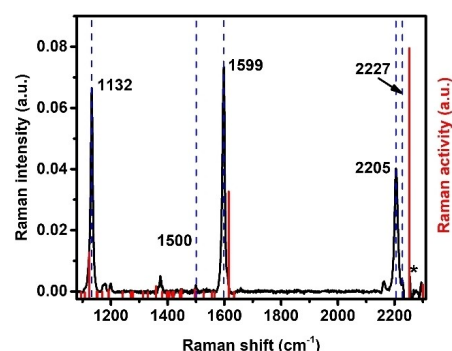


**Figure 3.** Steady-state Raman spectrum of DACN-DPA in MeCN; experimental (black, peaks marked with blue dashed lines) and computed Raman activity (red). The star represents a negative amplitude that arises as consequence of the subtraction error of the solvent's  $\text{C}\equiv\text{N}$  Raman band.

(vacuum) Raman spectra are shown in Figure S3, and the peak positions and corresponding vibrations are given in Table S2. The strong peaks at 2205  $\text{cm}^{-1}$ , 1600  $\text{cm}^{-1}$  and 1132  $\text{cm}^{-1}$  are assigned to the  $\text{C}\equiv\text{C}$  stretch, phenyl ring  $\text{C}=\text{C}$  stretch and a combination of vibrations of  $\text{CC}-\text{C}_{\text{ph}}$  and phenyl rings, respectively. The Raman band of the  $\text{C}\equiv\text{N}$  stretch in DACN-DPA appears at 2227  $\text{cm}^{-1}$  as a shoulder with a small amplitude, which is also depicted in Figure S3.

### Transient absorption (TA)

Femtosecond TA measurements of DACN-DPA were performed in *n*-hexane and MeCN, exciting at 345 nm in order to understand the effect of solvent polarity on the excited state dynamics. The TA spectra were measured in the range of 375–725 nm at various time delays that are shown in Figures 4 and 5 for both solvents. The corresponding 2D plots for both solvents are shown in Figure S4 in the Supporting Information.

In the case of *n*-hexane, post 200 fs of photoexcitation, an intense transient absorption band appears at ~510 nm along with a weaker shoulder at ~590 nm (Figure 4 (a)). The transient band at ~510 nm is assigned to the absorption from the Franck-Condon state to higher levels. Along with positive transient absorption bands, a negative band at ~400 nm could be attributed to the stimulated emission (SE) from the  $S_1$  state. For further time-delays of the probe beam, the intensity of the transient absorption bands increases until 25 ps while the peak positions remain the same. Such a feature is consistent with the structural relaxation of the Franck-Condon (FC) state while reaching a relaxed LE state similar to the observation in the case of bis(phenylethynyl)benzene.<sup>[68–70]</sup>

At longer time delays, as shown in Figure 4b, the excited-state absorption band exhibits a decrease in its amplitude along with the rise of a broad band centered at ~550 nm. The new band at ~550 nm does not show any decay even for a time-delay of ~1.8 ns, the maximum time delay in our experimental set up. It is also evident that there exist two isosbestic points at ~422 nm and ~542 nm, indicative of a single excited species that is evolving into long-lived species.

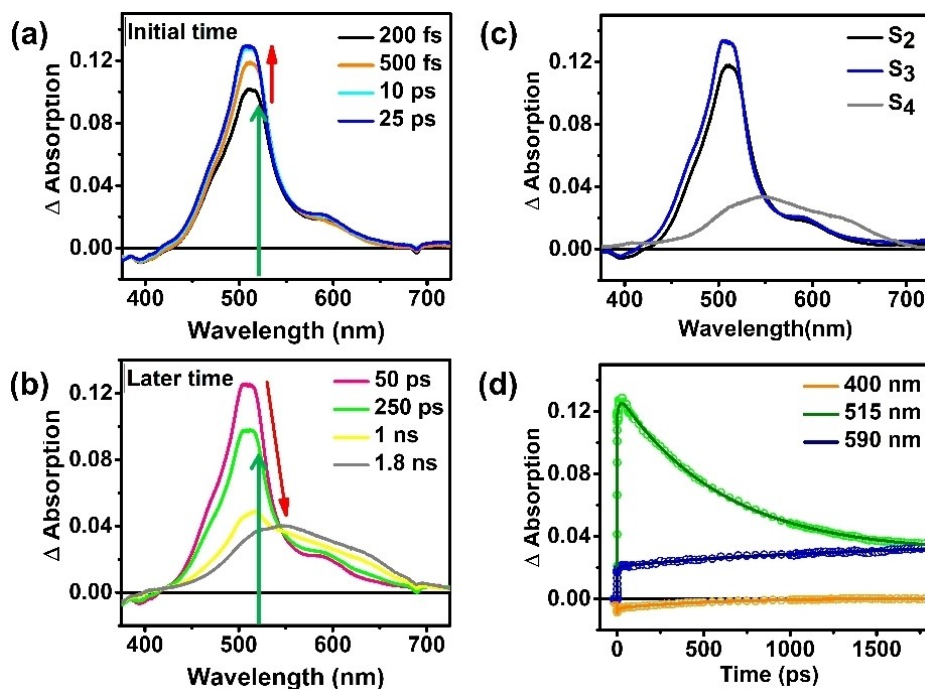


**Figure 4.** Transient absorption (TA) spectra of DACN-DPA in *n*-hexane (a) at shorter time window, (b) at longer time window, (c) corresponding species associated spectra (*S* in the insets stands for species), and (d) kinetic traces at selected wavelengths. The green arrow indicates the position of the Raman pump in URLs.

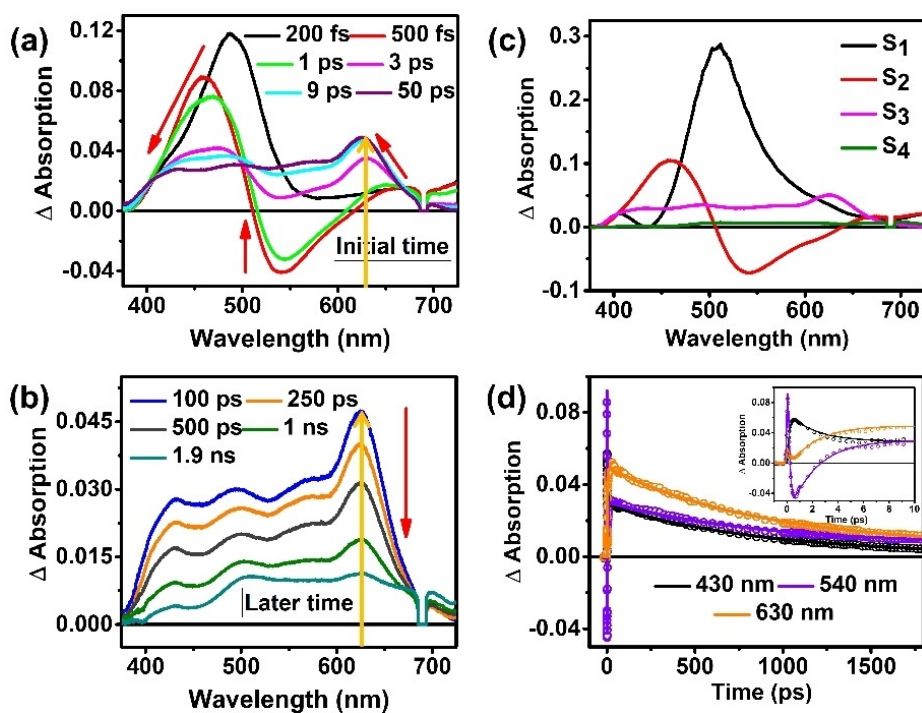


**Figure 5.** TA spectra of DACN-DPA in MeCN (a) at a shorter time window, (b) at a longer time window, (c) corresponding species associated spectra, and (d) kinetic traces at selected wavelengths. The yellow arrow indicates the position of the Raman pump in URLs.

Such a long-lived absorption band at ~550 nm is attributed to the  $T_n \leftarrow T_1$  transition.

In the case of MeCN, a polar aprotic solvent, the TA spectra exhibit a different trend in comparison with the non-polar

solvent. At a time delay of 200 fs, an excited-state absorption band appears at ~490 nm that corresponds to the Franck-Condon state, which subsequently exhibits a blueshift to ~445 nm at a time delay of ~500 fs. Furthermore, TA develops



a negative band centered at  $\sim 535$  nm that is attributed to stimulated emission (SE), as the spectral features match well with the steady-state emission spectrum. The new emissive state that forms on the time scale of  $\sim 500$  fs can be related to the ICT state, as it exhibits a large Stokes shift  $\sim 8700$   $\text{cm}^{-1}$  due to a greater stabilization by the polar solvent. At longer time delays, the transient absorption band at 445 nm exhibits a decay in intensity along with a blue shift, which can be correlated either to solvation or cooling process. The amplitude of the SE band decays to zero and a new band at 630 nm grows within a time scale of  $\sim 3$  ps. We assign such a 3 ps time scale to a structural distortion of the ICT state. Furthermore, such a distorted ICT state survives for a much longer time period and eventually decays back to the ground state on a time scale of  $\sim 900$  ps. These results are in good agreement with previously reported data.<sup>[55,56]</sup> We performed a global analysis of the TA data and obtained the time constants that are tabulated in Table 1. The experimental data can be well reproduced with four components in *n*-hexane and with three components in MeCN. The species associated spectra and the decay kinetic fits for selected probe wavelengths are shown in Figures 4 (c,d) and 5 (c,d), respectively. In the case of *n*-hexane solvent, the  $\tau_1$  component ( $< 150$  fs) is within our instrument resolution.  $\tau_2$  (13.4 ps) is assigned to structural relaxation or vibrational cooling, while  $\tau_3$  (614 ps) is assigned to the intersystem crossing (ISC) process. In the case of MeCN solvent,  $\tau_1$  ( $\sim 150$  fs) is within the instrument resolution. The  $\tau_2$  component (2.2 ps) is associated with the disappearance of the SE features along with the formation of a broad absorption feature from 400–650 nm. We assign this component to the evolution of the ICT state towards a distorted-ICT-type dark state, while the  $\tau_3$  component (878 ps) is assigned to the

lifetime of the dark distorted-ICT state rather than a ground state intermediate as it is highly correlated with the radiative lifetime of the large red-shifted emission in MeCN.<sup>[55,56]</sup> It is not immediately obvious how the structural changes take place during the evolution of the ICT and distorted-ICT states from the TA data analysis. We discuss these aspects in the next section using our URLS data analysis.

### Ultrafast Raman loss spectroscopy (URLS)

The broadband Raman probe (white light (WL)) possesses a higher-frequency spectrum with respect to the Raman pump in the case of URLS, while in femtosecond stimulated Raman spectroscopy (FSRS), WL consists of lower-frequency components. The Raman signals typically appear as loss (gain) features in the WL spectrum in URLS (FSRS). We primarily focus on elucidating the internal structural dynamics that occur within a time scale of 3 ps during the evolution of the ICT state to the distorted-ICT state. As there are several internal vibrational coordinates in DACN-DPA, we analyze those exhibiting a strong effect during the ICT to the distorted ICT state evolution using URLS measurements with high temporal and spectral resolutions.

**DACN-DPA in a non-polar environment:** Excited-state URLS spectra of DACN-DPA in *n*-hexane were measured by employing an actinic pump at 345 nm ( $\pi \rightarrow \pi^*$  transition), and a ps-Raman pump centered at 520 nm, which is in resonance with the TA band. The raw data from the URLS spectra were corrected by background subtraction and the processed spectra are presented in Figure 6. It is clear from Figure 6(a) that only two bands are apparent in this spectral region, i.e., an intense positive band centered at  $\sim 2078$   $\text{cm}^{-1}$  and a weak and dispersive band centered at  $\sim 1600$   $\text{cm}^{-1}$ . The positive and dispersive nature of the URLS peaks arises due to a complex resonance effect with the TA band. If the position (e.g.,  $\sim 2100$   $\text{cm}^{-1}$ ) of the Raman loss band is around the absorption maximum (TA, i.e.,  $\sim 470$  nm), such a band appears as a positive instead of a negative band. The reason for such a change in the

Table 1. TA kinetic parameters in <i>n</i> -hexane and MeCN obtained from global analysis.				
DACN-DPA	$\tau_1$	$\tau_2$	$\tau_3$	$\tau_4$
<i>n</i> -hexane	Ultrafast	13.4 ps	614 ps	Long-lived
MeCN	150 fs	2.2 ps	878 ps	–

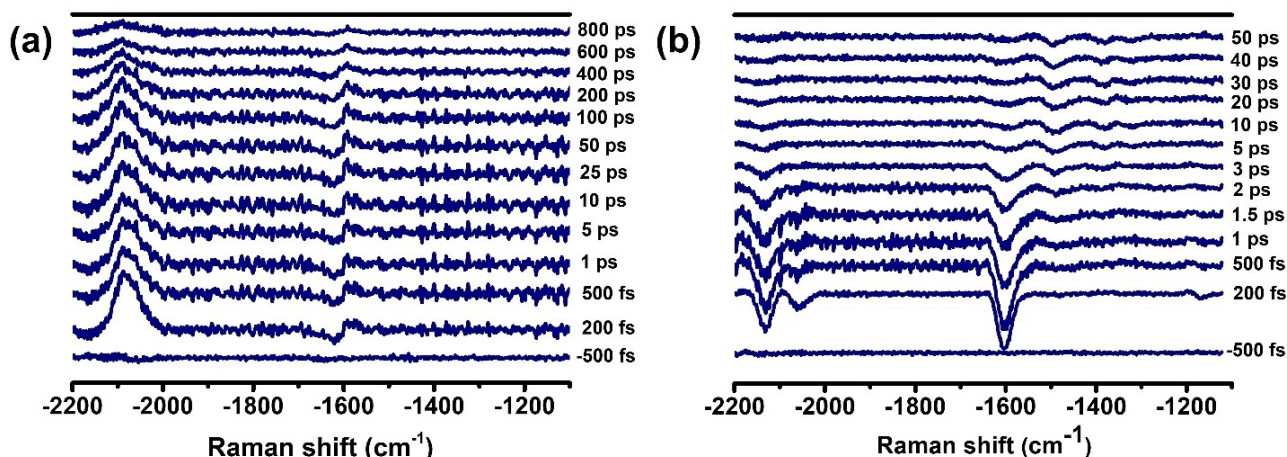


Figure 6. URLS spectra of DACN-DPA in (a) *n*-hexane, and (b) MeCN at different delay times.

Raman lineshape upon various Raman pump excitations is discussed in an earlier report.<sup>[71,72]</sup> Briefly, the Raman pump at 520 nm ( $19230\text{ cm}^{-1}$ ) and  $19230 + 2100\text{ cm}^{-1}$  corresponds to ca. 469 nm. The Raman band associated with the  $\text{C}\equiv\text{N}$  stretching mode in the excited state is not apparent due to its weaker Raman cross-section although it was observed in the ground state Raman spectrum ( $\sim 2227\text{ cm}^{-1}$ ) as shown in Figure 3. The tentative assignments for the URLS modes are presented in Table 2 based on DFT calculations and comparison with the ground state Raman spectrum.

The  $2078\text{ cm}^{-1}$  band is assigned to the  $\text{C}\equiv\text{C}$  stretch and the  $1600\text{ cm}^{-1}$  band is attributed to  $\text{C}=\text{C}$  stretching mode of the phenyl rings. The transient Raman band at  $2078\text{ cm}^{-1}$  is red shifted by  $\sim 127\text{ cm}^{-1}$  when compared to the ground state frequency at  $\sim 2205\text{ cm}^{-1}$ , reflecting the reduced bond order of the central  $\text{C}\equiv\text{C}$  bond. Interestingly, the  $\text{C}=\text{C}$  stretching frequency does not alter significantly from its ground state frequency. These two modes possess essential information about the molecular structure. The intensity ratio of the  $\text{C}\equiv\text{C}$  and  $\text{C}=\text{C}$  modes in the excited state is reversed with respect to the ground state for which the  $\text{C}=\text{C}$  mode is more intense. Upon resonant excitation, the relative displacement of the modes significantly influences the Raman intensity, i.e., the higher the displacement, the higher will be the Raman intensity. Furthermore, the totally symmetric modes exhibit significant enhancement upon resonant excitation. A relatively lower intensity of the  $\text{C}=\text{C}$  mode (phenyl ring stretch), possibly indicates that this mode undergoes very little structural distortion upon photoexcitation. This is supported by the fact that there is no formation of a charge transfer state in *n*-

hexane, i.e., the electron density on the phenyl rings remains unaffected by the photoexcitation.

The kinetics of the integrated peak area and the peak position of the Raman band at  $2078\text{ cm}^{-1}$  are shown in Figures 7(a) and 7(b), respectively. The peak area kinetics exhibits a rapid decay in the ultrafast time scale followed by a growth in the amplitude for a time delay of  $\sim 30\text{ ps}$ . For further time delays, the amplitude exhibits a slow decay with a single exponential. On the other hand, the peak position of the  $\text{C}\equiv\text{C}$  stretch exhibits a rapid red shift on the ultrafast time scale followed by a blue shift with fast and slow components at  $\sim 20\text{ ps}$  and  $\sim 600\text{ ps}$ , respectively. We fitted the data by fixing the long-time component at  $\sim 600\text{ ps}$  to avoid the large error limit due to the overall time-window of the experiment i.e.,  $\sim 1.80\text{ ns}$ . In order to comprehend the excited-state dynamics, we performed theoretical calculations on the ground-state by scanning the dihedral angle for the phenyl ring twist of DACN-DPA from  $0^\circ$ – $180^\circ$  in steps of  $20^\circ$  as depicted in Figure S6. At room temperature, conformers with a twist angle of up to  $\sim 45^\circ$  are accessible as shown in Figure S7. Therefore, all rotamers up to  $\sim 45^\circ$  twists can be electronically excited with the pump wavelength at  $345\text{ nm}$ . The intensity rise that occurs within  $\sim 30\text{ ps}$  and, therefore, is tentatively assigned to the combined effect of vibrational cooling and planarization processes. The kinetic plot of the amplitude of the Raman mode at  $2078\text{ cm}^{-1}$  is shown in Figure 7(a). The plot is the best fit with a tri-exponential fit yielding time constants of  $\tau_1 = 350 \pm 30\text{ fs}$ ,  $\tau_2 = 29 \pm 2\text{ ps}$ , and  $\tau_3 = 435 \pm 30\text{ ps}$ . The ultrafast decay component  $\tau_1$  is attributed to the formation of an electronically delocalized, relaxed non-planar, non-equilibrated state from the initially formed FC state. Subsequent to such relaxation, the population

**Table 2.** Peak assignments of the experimental Raman bands for the ground and the excited states in *n*-hexane/MeCN.

Ground state experimental Raman frequency [ $\text{cm}^{-1}$ ]	Excited state experimental Raman frequency [ $\text{cm}^{-1}$ ]	Tentative assignments
2228/2227	–	$\text{C}\equiv\text{N}$ stretch
2209/2205	2078/2131	$\text{C}\equiv\text{C}$ stretch
2162/2160	2058	First overtone of $1132\text{ cm}^{-1}$ mode
1599/1599	1600/1600	$\text{C}=\text{C}$ Ring stretching
1498/1500	1492	$\text{C}_{\text{ph}}-\text{CN} + \text{C}_{\text{ph}}-\text{CC} + \text{C}_{\text{ph}}-\text{NMe}_2$ stretching motion
1132/1132	–	Ring breathing + $\text{C}_{\text{ph}}-\text{CC}$ stretching

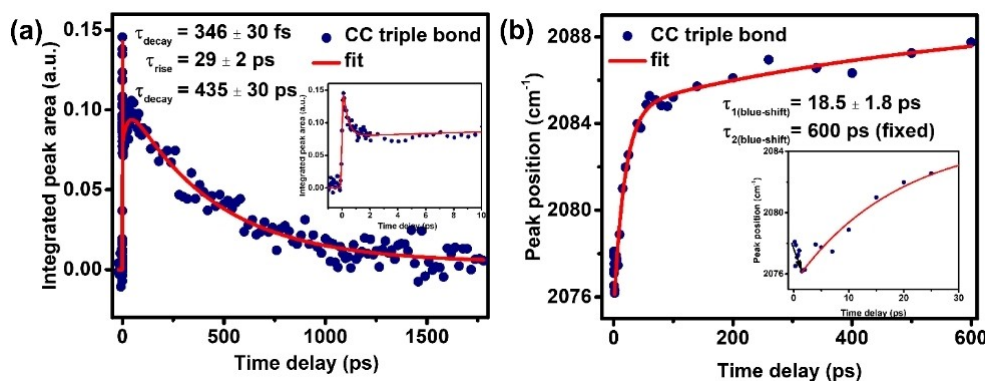


**Figure 7.** Kinetics of the excited state  $\text{C}\equiv\text{C}$  stretch of DACN-DPA in *n*-hexane. (a) Kinetics of integrated peak area of  $\text{C}\equiv\text{C}$  stretch, and (b) kinetics of the peak position of  $\text{C}\equiv\text{C}$  stretch. (Blue dots: experimental data; red line: fit curve). Insets in the Figures represent the corresponding kinetics at the early time window.

evolves towards a more stable planar geometry while undergoing vibrational cooling with a time constant of  $\tau_2$ . The longer time constant  $\tau_3$  is attributed to the ISC process along with cooling process from the equilibrated LE state to the hot triplet state.

During the formation of the electronically delocalized state, the C $\equiv$ C stretch exhibits a red shift of  $\sim 2\text{ cm}^{-1}$  in the ultrafast time-scale as shown in Figure 7(b). Upon reaching a value of  $\sim 2076\text{ cm}^{-1}$ , it undergoes a blue shift of ca.  $10\text{ cm}^{-1}$  with a time scale of  $\sim 20\text{ ps}$ . Such a time scale matches well with the time constant obtained from the global analysis of the TA data. Interestingly, the Raman band of the C $\equiv$ C stretch exhibits a further slow blue shift which could be attributed to the formation of the triplet state and vibrational cooling of the hot excited triplet state.

**DACN-DPA in a polar environment:** Excited-state URLs spectra of DACN-DPA in MeCN were measured by employing an actinic pump at 345 nm and a Raman pump at 630 nm that is in resonance with the TA band as shown in Figure 5(a,b). The choice of the Raman pump at this region is motivated by the fact that we wish to unravel the structural changes associated with the evolution of a charge separation event. The URLs spectra at selected time-delays in MeCN are presented in Figure 6(b). The transient URLs spectrum at 200 fs is characterized by two strong vibrational modes at  $\sim 2131\text{ cm}^{-1}$  and  $\sim 1600\text{ cm}^{-1}$  along with two weaker bands at  $\sim 2058\text{ cm}^{-1}$  and  $\sim 1183\text{ cm}^{-1}$ . We assign the  $2131\text{ cm}^{-1}$  and  $1600\text{ cm}^{-1}$  bands to the C $\equiv$ C stretch and to the C=C stretch of the phenyl rings, respectively. The intensity of the C $\equiv$ C and C=C bands exhibit a rapid decay on a time scale of 5 ps. The formation of two new

long-lived modes at  $\sim 1492\text{ cm}^{-1}$  and  $\sim 1385\text{ cm}^{-1}$  is very apparent, clearly reflecting the formation of a new state. Comparison of these bands with the ground-state Raman bands and their tentative assignments are presented in Table 2. It is interesting to note that the C=C stretch is the strongest Raman band in the excited state in the case of MeCN, which is in contrast to the case of *n*-hexane. This is also consistent with the assumption that significant bond displacement is associated with phenyl ring stretches as a consequence of a prominent charge transfer process in polar solvents.

The kinetics of integrated peak area and peak position for a few Raman modes are shown in Figure 8. The kinetics of the integrated peak area for both the C $\equiv$ C and C=C modes are best fitted with a mono-exponential decay, while the  $1492\text{ cm}^{-1}$  mode is best fitted with a mono-exponential rise time component. The time constants are observed to be within 1.5 ps. Interestingly, the values of these time constants are in agreement with our TA results. Based on these observations, such a time constant is essentially attributed to the formation of a distorted-ICT state. Interestingly, during such an ultrafast time-scale, the C $\equiv$ C and C=C modes show an increase in their peak area amplitudes and a red shift in their corresponding peak positions. The initial increase in the intensity occurs due to a charge transfer process and, during the charge separation process, the bond order is expected to decrease; as a consequence, it leads to a red shift in the vibrational band positions. However, in the next  $\sim 2\text{ ps}$  time delay, both peaks show a rapid decay in their peak intensities while the peak positions show an interesting trend.

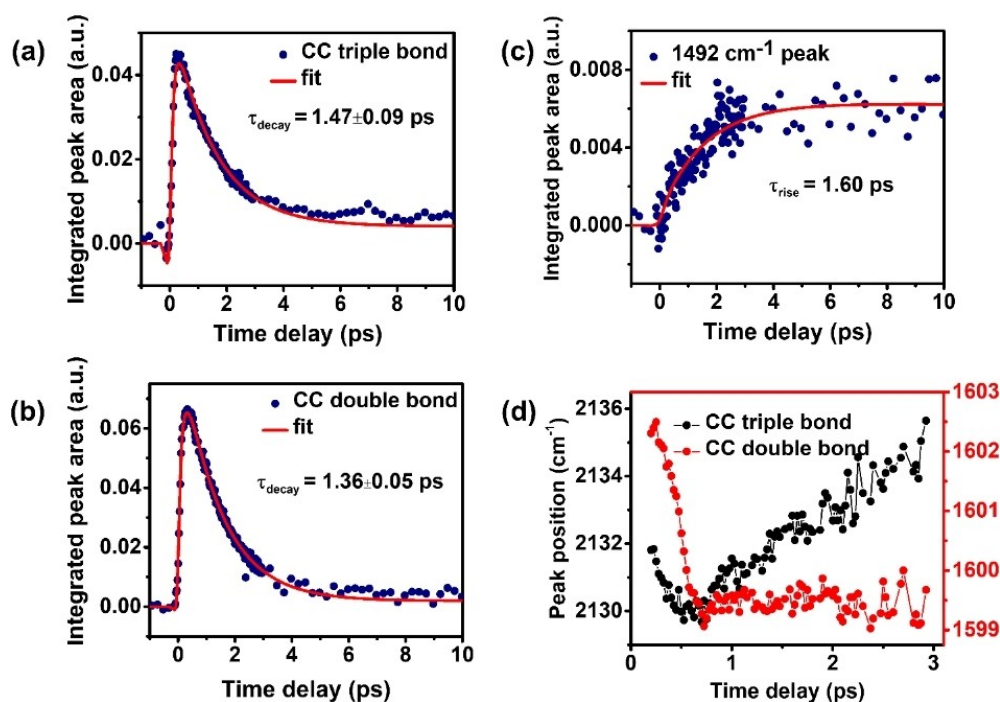


**Figure 8.** Kinetics of the excited state Raman modes of DACN-DPA in MeCN (blue dots: experimental data and red line: corresponding fit). Kinetics of the integrated peak area of (a) C $\equiv$ C mode, (b) C=C, (c)  $1492\text{ cm}^{-1}$ , and (d) comparison of the kinetics of the peak positions of the C $\equiv$ C (black) and C=C bands (red) in the early time window.



The kinetics of the peak position of the  $2131\text{ cm}^{-1}$  and  $1600\text{ cm}^{-1}$  bands are shown in Figure 8(d). The  $2131\text{ cm}^{-1}$  band is red shifted by  $74\text{ cm}^{-1}$  in comparison with the corresponding ground state peak position at  $2205\text{ cm}^{-1}$ , while the  $\text{C}=\text{C}$  band appears to be a little blue shifted with respect to the ground state Raman band. This indicates that the  $\pi\pi^*$  transition has a significant effect on the  $\text{C}\equiv\text{C}$  stretch; as the electron shifts to the anti-bonding orbital, it leads to a decrease in the bond order while the  $\text{C}=\text{C}$  frequency exhibits little change. In the time period of 1 ps, the  $\text{C}\equiv\text{C}$  and  $\text{C}=\text{C}$  stretches exhibit a red-shift of  $\sim 2\text{ cm}^{-1}$  and  $\sim 5\text{ cm}^{-1}$ , respectively, clearly indicating the charge transfer process occurring on such timescale. In the next  $\sim 3\text{ ps}$  period, the  $\text{C}\equiv\text{C}$  stretch exhibits a blue shift, while the  $\text{C}=\text{C}$  stretch exhibits a negligible shift in its peak position. These features clearly demonstrate that the response of the phenyl rings towards the distortion in the structure is different from that of the  $\text{C}\equiv\text{C}$  stretch. The initial blue shift in the peak position is due to the rotation of one of the phenyl rings attached to the  $\text{C}\equiv\text{C}$  entity to produce a planar structure.

Upon completion of the charge transfer process, the central  $\text{CC}-\text{C}_{\text{ph}}$  unit acquires an 'allene character' as proposed by

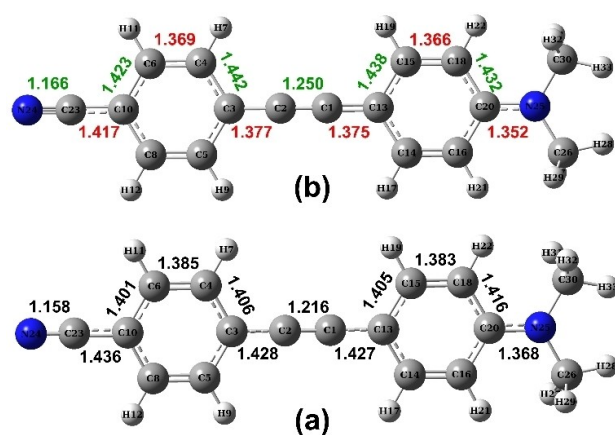


**Figure 9.** Optimized geometries with bond lengths (Å) of DACN-DPA in MeCN in (a) the ground state and (b) the excited state with increased (green) and decreased (red) bond lengths.

**Table 3.** Comparison of the calculated bond lengths (Å) of the optimized geometries of DACN-DPA in MeCN for the ground and excited states.

Bonds	Ground state [Å]	Excited state [Å]
C1–C2	1.216	1.250
C2–C3	1.428	1.377
C3–C4	1.406	1.442
C3–C5	1.406	1.442
C4–C6	1.385	1.369
C6–C10	1.401	1.423
C8–C10	1.401	1.423
C1–C13	1.427	1.375
C13–C14	1.405	1.438
C13–C15	1.405	1.438
C14–C16	1.383	1.366
C16–C20	1.416	1.432
C18–C20	1.416	1.432
C10–C23	1.436	1.417
C23–N24	1.158	1.166
C20–N25	1.368	1.352

Vauthey and coworkers,<sup>[61]</sup> with the appearance of new peaks. Upon formation, such a hot TICT state undergoes vibrational cooling and leads to a further, slower blue shift of the  $\text{C}\equiv\text{C}$  stretch. However, our TD-DFT calculations predict the formation of a planar structure after the charge separation, as shown in Figure 9. Furthermore, a comparison of the bond lengths in both the ground and the excited-states, as given in Table 3, indicates that the  $\text{C}\equiv\text{C}$  and  $\text{C}\equiv\text{N}$  bond along with C3–C4, C3–C5, C6–C10, C8–C10, C13–C14, C13–C15, C16–C20, C18–C20 bond lengths increase in the excited state while the other bond lengths decrease. This clearly indicates that the migration of charge from the donor to the acceptor has a significant effect on the bond lengths and their strengths. Such dynamics are also well-supported by our URLs results.

## Conclusion

In summary, we used fs-TA and time-resolved URLs methods to examine the excited state ICT process in DACN-DPA in *n*-hexane and acetonitrile environments. The fs-TA measurements in *n*-hexane exhibits an ESA band at  $\sim 520\text{ nm}$  with a predominantly longer lifetime ( $> 2\text{ ns}$ ), while in acetonitrile ESA occurs at  $\sim 630\text{ nm}$  with a shorter lifetime ( $\sim 1.5\text{ ps}$ ), clearly demonstrating distinct excited state dynamics in these solvents. The fs-URLS measurements in *n*-hexane show Raman bands at  $\sim 2076\text{ cm}^{-1}$  ( $\text{C}\equiv\text{C}$  stretch) and a weak dispersive mode at  $1600\text{ cm}^{-1}$  ( $\text{C}=\text{C}$  stretch) that decay with a time constant of  $\sim 500\text{ ps}$ . In the case of acetonitrile, Raman modes appear at  $2131\text{ cm}^{-1}$  ( $\text{C}\equiv\text{C}$  stretch) and  $1600\text{ cm}^{-1}$  ( $\text{C}=\text{C}$  stretch) with a lifetime of  $\sim 1.5\text{ ps}$  along with growth of a new Raman band at  $\sim 1492\text{ cm}^{-1}$  on a similar time scale, a clear indication of a prominent structural modification associated with the intramolecular charge transfer. A thorough analysis of the TD-DFT data also corroborates the experimentally observed structural changes that arise as a consequence of the intramolecular charge transfer and predicts a planar excited-state structure after charge transfer, rather than a TICT state. URLs measurements in synergy with other ultrafast studies enabled the unravelling of the underlying intricate structural dynamics that govern the efficacy and extent of the intramolecular charge transfer dynamics in DACN-DPA, a donor- $\pi$ -bridge-acceptor system.

## Experimental Section

DACN-DPA, a light yellow powder, was synthesized according to a literature procedure<sup>[73]</sup> and the purity of the sample was confirmed by  $^1\text{H-NMR}$  and  $^{13}\text{C-NMR}$  spectroscopy (see Supporting Information). The MeCN, DCM and *n*-hexane solvents used for the experiments were of HPLC grade obtained from Sigma Aldrich.

**Computational methods.** All calculations reported herein were performed using the Gaussian 09 (G09)<sup>[74]</sup> suite. The ground state DFT optimization at the  $\text{C}_s$  geometry and frequency calculations were performed using the CAM-B3LYP/cc-pVDZ functional and basis set.<sup>[75–77]</sup> The CAM-B3LYP functional is a range-separated hybrid that includes a distance-dependent mixing Hartree-Fock



exchange and Becke 1988 exchange with the hybrid B3LYP exchange-correlation functional to provide an improved description of CT transitions and states.<sup>[77,78]</sup> Solvent effects were included in the DFT and TD-DFT calculations using integral equation formalism-polarizable continuum solvent model as employed in the G09 suite.<sup>[79–81]</sup> No negative frequencies were obtained for the ground state optimization indicating that optimized geometries correspond to local minima. The excited-state structure of DACN-DPA was optimized using TD-DFT with the same method as employed for the ground state. TD-DFT calculations using the CAM-B3LYP functional were performed to obtain the vertical excitation energies and electron density difference map (EDDM).<sup>[82,83]</sup> The computed vibrational spectra were plotted using GaussSum v2.2.6 software<sup>[84]</sup> and scaled with a factor of 0.962.<sup>[85]</sup> The structural depiction and molecular orbitals were generated by using the GaussView 6.0 visualization program.

**Experimental methods.** Steady-state absorption measurements were performed using a Shimadzu UV-2600 absorption spectrophotometer. Fluorescence measurements were carried out with a Horiba Fluoromax-4 spectrofluorometer. Steady-state Raman spectra were measured using a Renishaw micro-Raman spectrometer, exciting at 785 nm.

Femtosecond transient absorption (TA) and Ultrafast Raman Loss Spectroscopy (URLS) measurements were performed using a home-built experimental set up. Briefly, the regenerative amplifier (Spitfire Pro, Spectra Physics) produces ultrashort laser pulses with a pulse width of ~100 fs, centered at ~780 nm, a pulse energy of ~2 mJ and a repetition rate of 1 kHz. The output is split into two equal parts. One part is used to pump an OPA (Spectra-Physics) to generate laser pulses centered at ~630 nm (~40 μJ) and at ~520 nm (~70 μJ), which are further converted into a ~ps pulse (~20 cm<sup>-1</sup>) by a spectral filter assembly for Raman pump excitation. The other 1 mJ portion is further split 95:5, where 95% is used to pump a TOPAS-C (Light conversion, Spectra-Physics) laser to produce pulses in the UV- range for actinic pump excitation. A small portion of remaining 5% of the energy is allowed to pass through a CaF<sub>2</sub> crystal and a sapphire crystal to generate essentially white-light supercontinuum pulses for fs-TA and URLS experiments. The white-light continuum is further split into two parts to be used as the probe and reference beams.

The concentration of the sample solution was 200 μM. We employed a flow-cell with a pathlength of 0.5 mm for the time-resolved Raman experiments with Raman pump energies of ~400 nJ (520 nm) and ~300 nJ (630 nm) per pulse. TA measurements were performed using a magic angle geometry between the pump and probe beam polarizations, while for URLS measurements, the pump and probe were maintained at the same polarization.

## Acknowledgements

S.U. acknowledges the Department of Science and Technology (DST) for a J.C. Bose fellowship. A.B. and N.D. thank the Council of Scientific and Industrial Research (CSIR), and the DST for financial assistance. A.B. and N.D. thank Dr. Surajit Kayal for help in interpreting the data. We thank Ms. Andrea Reichert at the Julius-Maximilians-University Würzburg for help with synthesis of the DACN-DPA sample. T.B.M. thanks the Julius-Maximilians-Universität Würzburg for support. F.S. thanks the Julius-Maximilians-Universität Würzburg and the DAAD for a PROMOS fellowship. Y.A.L. acknowledges the Science and Engineering Research Board

(SERB) for financial support, through grant no. CRG/2020/000321. Open Access funding enabled and organized by Projekt DEAL.

## Conflict of Interest

The authors declare no conflict of interest.

## Data Availability Statement

The data that support the findings of this study are available in the supplementary material of this article.

**Keywords:** charge transfer · ultrafast Raman loss spectroscopy · 4-dimethylamino-4'-cyanodiphenylacetylene · transient absorption · TD-DFT

- [1] R. A. Marcus, N. Sutin, *Biochim. Biophys. Acta Bioenerg.* **1985**, *811*, 265–322.
- [2] G. Sedghi, K. Sawada, L. J. Esdaile, M. Hoffmann, H. L. Anderson, D. Bethell, W. Haiss, S. J. Higgins, R. J. Nichols, *J. Am. Chem. Soc.* **2008**, *130*, 8582–8583.
- [3] R. E. Blankenship, *Molecular Mechanisms of Photosynthesis*, John Wiley & Sons, Hoboken, NJ **2021**.
- [4] S. E. Shaheen, B. Kippelen, N. Peyghambarian, J.-F. Wang, J. D. Anderson, E. A. Mash, P. A. Lee, N. R. Armstrong, Y. Kawabe, *J. Appl. Phys.* **1999**, *85*, 7939–7945.
- [5] B. Daly, J. Ling, A. P. De Silva, *Chem. Soc. Rev.* **2015**, *44*, 4203–4211.
- [6] M. Grätzel, *Acc. Chem. Res.* **2009**, *42*, 1788–1798.
- [7] J.-L. Brédas, J. P. Calbert, D. A. da Silva Filho, J. Cornil, *Proc. Nat. Acad. Sci.* **2002**, *99*, 5804–5809.
- [8] R. Métivier, R. Amengual, I. Leray, V. Michelet, J.-P. Genêt, *Org. Lett.* **2004**, *6*, 739–742.
- [9] P. Nguyen, G. Lesley, T. B. Marder, I. Ledoux, J. Zyss, *Chem. Mater.* **1997**, *9*, 406–408.
- [10] A. Weller, *Z. Phys. Chem.* **1982**, *133*, 93–98.
- [11] E. Lippert, W. Lüder, F. Moll, W. Nägele, H. Boos, H. Prigge, I. Seibold-Blankenstein, *Angew. Chem.* **1961**, *73*, 695–706.
- [12] E. Lippert, W. Rettig, V. Bonacic-Koutecky, F. Heisel, J. A. Miehe, *Adv. Chem. Phys.* **1987**, *68*, 1–173.
- [13] S. I. Druzhinin, P. Mayer, D. Stalke, R. von Bülow, M. Noltemeyer, K. A. Zachariasse, *J. Am. Chem. Soc.* **2010**, *132*, 7730–7744.
- [14] W. M. Kwok, C. Ma, P. Matousek, A. W. Parker, D. Phillips, W. T. Toner, M. Towrie, S. Umaphathy, *J. Phys. Chem. A* **2001**, *105*, 984–990.
- [15] C. Ma, W. M. Kwok, P. Matousek, A. W. Parker, D. Phillips, W. T. Toner, M. Towrie, *J. Phys. Chem. A* **2002**, *106*, 3294–3305.
- [16] J. M. Rhinehart, J. R. Challa, D. W. McCamant, *J. Phys. Chem. B* **2012**, *116*, 10522–10534.
- [17] Y. Zhao, W. Liang, *Chem. Soc. Rev.* **2012**, *41*, 1075–1087.
- [18] E. R. Barthel, I. B. Martini, B. J. Schwartz, *J. Phys. Chem. B* **2001**, *105*, 12230–12241.
- [19] L. Serrano-Andres, M. Merchán, B. O. Roos, R. Lindh, *J. Am. Chem. Soc.* **1995**, *117*, 3189–3204.
- [20] R. Misra, S. P. Bhattacharyya, *Intramolecular Charge Transfer: Theory and Applications*, John Wiley & Sons, Weinheim **2018**.
- [21] Z. R. Grabowski, K. Rotkiewicz, W. Rettig, *Chem. Rev.* **2003**, *103*, 3899–4032.
- [22] K. A. Zachariasse, S. I. Druzhinin, S. A. Kovalenko, T. Senyushkina, *J. Chem. Phys.* **2009**, *131*, 224313.
- [23] A. Demeter, S. Druzhinin, M. George, E. Haselbach, J.-L. Roulin, K. A. Zachariasse, *Chem. Phys. Lett.* **2000**, *323*, 351–360.
- [24] K. A. Zachariasse, M. Grobys, *J. Photochem. Photobiol. A* **1997**, *105*, 373–383.
- [25] A. Steffen, M. G. Tay, A. S. Batsanov, J. A. K. Howard, A. Beeby, K. Q. Vuong, X. Sun, M. W. George, T. B. Marder, *Angew. Chem. Int. Ed.* **2010**, *49*, 2349–2353; *Angew. Chem.* **2010**, *122*, 2399–2403.

- [26] P. Nguyen, Z. Yuan, L. Agocs, G. Lesley, T. B. Marder, *Inorg. Chim. Acta* **1994**, 220, 289–296.
- [27] J. S. Siddle, R. M. Ward, J. C. Collings, S. R. Rutter, L. Porrès, L. Applegarth, A. Beeby, A. S. Batsanov, A. L. Thompson, J. A. K. Howard, *New J. Chem.* **2007**, 31, 841–851.
- [28] B. Albinsson, M. P. Eng, K. Pettersson, M. U. Winters, *Phys. Chem. Chem. Phys.* **2007**, 9, 5847–5864.
- [29] J. Zyss, I. Ledoux, S. Volkov, V. Chernyak, S. Mukamel, G. P. Bartholomew, G. C. Bazan, *J. Am. Chem. Soc.* **2000**, 122, 11956–11962.
- [30] W. Akemann, D. Laage, P. Plaza, M. M. Martin, M. Blanchard-Desce, *J. Phys. Chem. B* **2008**, 112, 358–368.
- [31] S. Arzhantsev, K. A. Zachariasse, M. Maroncelli, *J. Phys. Chem. A* **2006**, 110, 3454–3470.
- [32] T. M. Fasina, J. C. Collings, D. P. Lydon, D. Albesa-Jové, A. S. Batsanov, J. A. K. Howard, P. Nguyen, M. Bruce, A. J. Scott, W. Clegg, *J. Mater. Chem.* **2004**, 14, 2395–2404.
- [33] G. L. Closs, J. R. Miller, *Science* **1988**, 240, 440–447.
- [34] B. Albinsson, J. Mårtensson, *J. Photochem. Photobiol. C* **2008**, 9, 138–155.
- [35] T. M. Fasina, J. C. Collings, J. M. Burke, A. S. Batsanov, R. M. Ward, D. Albesa-Jové, L. Porrès, A. Beeby, J. A. K. Howard, A. J. Scott, *J. Mater. Chem.* **2005**, 15, 690–697.
- [36] J. C. Collings, A. C. Parsons, L. Porrès, A. Beeby, A. S. Batsanov, J. A. K. Howard, D. P. Lydon, P. J. Low, I. J. S. Fairlamb, T. B. Marder, *Chem. Commun.* **2005**, 2666–2668.
- [37] V. Karunakaran, S. Das, *J. Phys. Chem. B* **2016**, 120, 7016–7023.
- [38] A. Beeby, K. Findlay, P. J. Low, T. B. Marder, *J. Am. Chem. Soc.* **2002**, 124, 8280–8284.
- [39] C. Joachim, J. K. Gimzewski, A. Aviram, *Nature* **2000**, 408, 541–548.
- [40] A. S. Blum, J. G. Kushmerick, D. P. Long, C. H. Patterson, J. C. Yang, J. C. Henderson, Y. Yao, J. M. Tour, R. Shashidhar, B. R. Ratna, *Nat. Mater.* **2005**, 4, 167–172.
- [41] H. Amini, Ž. Ban, M. Ferger, S. Lorenzen, F. Rauch, A. Friedrich, I. Crnolatac, A. Kendel, S. Miljanić, I. Piantanida, *Chem. Eur. J.* **2020**, 26, 6017–6028.
- [42] M. Ferger, Ž. Ban, I. Krošl, S. Tomić, L. Dietrich, S. Lorenzen, F. Rauch, D. Sieh, A. Friedrich, S. Griesbeck, *Chem. Eur. J.* **2021**, 27, 5142–5159.
- [43] M. Biswas, P. Nguyen, T. B. Marder, L. R. Khundkar, *J. Phys. Chem. A* **1997**, 101, 1689–1695.
- [44] M. Szyzkowska, I. Bylińska, W. Wicz, *J. Photochem. Photobiol. A* **2016**, 326, 76–88.
- [45] M. Wierzbicka, I. Bylińska, C. Czaplewski, W. Wicz, *RSC Adv.* **2015**, 5, 29294–29303.
- [46] T. Ishibashi, H. Hamaguchi, *J. Phys. Chem. A* **1998**, 102, 2263–2269.
- [47] T. Ishibashi, H. Hamaguchi, *Chem. Phys. Lett.* **1997**, 264, 551–555.
- [48] H. Hiura, H. Takahashi, *J. Phys. Chem.* **1992**, 96, 8909–8915.
- [49] Y. Hirata, T. Okada, T. Nomoto, *Chem. Phys. Lett.* **1993**, 209, 397–402.
- [50] Y. Hirata, T. Okada, N. Mataga, T. Nomoto, *J. Phys. Chem.* **1992**, 96, 6559–6563.
- [51] K. Okuyama, T. Hasegawa, M. Ito, N. Mikami, *J. Phys. Chem.* **1984**, 88, 1711–1716.
- [52] M. Krämer, U. H. F. Bunz, A. Dreuw, *J. Phys. Chem. A* **2017**, 121, 946–953.
- [53] L. R. Khundkar, A. E. Stiegman, J. W. Perry, *J. Phys. Chem.* **1990**, 94, 1224–1226.
- [54] A. Broo, *Chem. Phys.* **1994**, 183, 85–94.
- [55] Y. Hirata, T. Okada, T. Nomoto, *Chem. Phys. Lett.* **1997**, 278, 133–138.
- [56] T. Fujiwara, M. Z. Zgierski, E. C. Lim, *J. Phys. Chem. A* **2011**, 115, 586–592.
- [57] M. Z. Zgierski, E. C. Lim, *Chem. Phys. Lett.* **2004**, 393, 143–149.
- [58] M. Z. Zgierski, T. Fujiwara, E. C. Lim, *Acc. Chem. Res.* **2010**, 43, 506–517.
- [59] Y. Amatatsu, *J. Phys. Chem. A* **2010**, 114, 543–551.
- [60] A. Amini, A. Harriman, *Phys. Chem. Chem. Phys.* **2003**, 5, 1344–1351.
- [61] B. Dereka, D. Svehkarev, A. Rosspeintner, M. Tromayer, R. Liska, A. M. Mohs, E. Vauthey, *J. Am. Chem. Soc.* **2017**, 139, 16885–16893.
- [62] J. Kubicki, M. Lorenc, P. Cochevin, O. Mongin, A. Amar, A. Boucekkin, A. Gaje, M. G. Humphrey, M. Morshedi, S. Lorenzen, F. Rauch, C. Scheufler, T. B. Marder, F. Paul, *J. Phys. Chem. C* **2020**, 124, 9755–9764.
- [63] R. Berera, R. van Grondelle, J. Kennis, *Photosynth. Res.* **2009**, 101, 105–118.
- [64] U. Harbola, S. Umapathy, S. Mukamel, *Phys. Rev. A* **2013**, 88, 11801.
- [65] N. K. Rai, A. Y. Lakshman, V. V. Nambodiri, S. Umapathy, *J. Chem. Sci.* **2012**, 124, 177–186.
- [66] B. Mallick, A. Lakshman, S. Umapathy, *J. Raman Spectrosc.* **2011**, 42, 1883–1890.
- [67] S. Umapathy, A. Lakshman, B. Mallick, *J. Raman Spectrosc.* **2009**, 40, 235–237.
- [68] A. Beeby, K. S. Findlay, P. J. Low, T. B. Marder, P. Matousek, A. W. Parker, S. R. Rutter, M. Towrie, *Chem. Commun.* **2003**, 3, 2406–2407.
- [69] K. Roy, S. Kayal, V. Ravi Kumar, A. Beeby, F. Ariese, S. Umapathy, *J. Phys. Chem. A* **2017**, 121, 6538–6546.
- [70] K. Roy, S. Kayal, F. Ariese, A. Beeby, S. Umapathy, *J. Chem. Phys.* **2017**, 146, 64303.
- [71] S. Umapathy, B. Mallick, A. Lakshman, *J. Chem. Phys.* **2010**, 133, 24505.
- [72] Z. Sun, J. Lu, D. H. Zhang, S.-Y. Lee, *J. Chem. Phys.* **2008**, 128, 144114.
- [73] E. J. Donckele, A. D. Finke, L. Ruhlmann, C. Boudon, N. Trapp, F. Diederich, *Org. Lett.* **2015**, 17, 3506–3509.
- [74] M. J. Frisch, G. W. Trucks, H. B. Schlegel, G. E. Scuseria, M. A. Robb, J. R. Cheeseman, G. Scalmani, V. Barone, B. Mennucci, G. A. Petersson, H. Nakatsuji, M. Caricato, X. Li, H. P. Hratchian, A. F. Izmaylov, J. Bloino, G. Zheng, J. L. Sonnenberg, M. Hada, M. Ehara, K. Toyota, R. Fukuda, J. Hasegawa, M. Ishida, T. Nakajima, Y. Honda, O. Kitao, H. Nakai, T. Vreven, J. A. Montgomery Jr., J. E. Peralta, F. Ogliaro, M. Bearpark, J. J. Heyd, E. Brothers, K. N. Kudin, V. N. Staroverov, T. Keith, R. Kobayashi, J. Normand, K. Raghavachari, A. Rendell, J. C. Burant, S. S. Iyengar, J. Tomasi, M. Cossi, N. Rega, J. M. Millam, M. Klene, J. E. Knox, J. B. Cross, V. Bakken, C. Adamo, J. Jaramillo, R. Gomperts, R. E. Stratmann, O. Yazyev, A. J. Austin, R. Cammi, C. Pomelli, J. W. Ochterski, R. L. Martin, K. Morokuma, V. G. Zakrzewski, G. A. Voth, P. Salvador, J. J. Dannenberg, S. Dapprich, A. D. Daniels, O. Farkas, J. B. Foresman, J. V. Ortiz, J. Cioslowski, D. J. Fox, *Gaussian 09, Revision D.01*, Gaussian, Inc., Wallingford CT **2013**.
- [75] T. H. Dunning Jr., *J. Chem. Phys.* **1989**, 90, 1007–1023.
- [76] S. Grimme, J. Antony, S. Ehrlich, H. Krieg, *J. Chem. Phys.* **2010**, 132, 154104.
- [77] T. Yanai, D. P. Tew, N. C. Handy, *Chem. Phys. Lett.* **2004**, 393, 51–57.
- [78] C. Adamo, D. Jacquemin, *Chem. Soc. Rev.* **2013**, 42, 845–856.
- [79] E. Cancès, B. Mennucci, J. Tomasi, *J. Chem. Phys.* **1997**, 107, 3032–3041.
- [80] J. Tomasi, B. Mennucci, R. Cammi, *Chem. Rev.* **2005**, 105, 2999–3094.
- [81] G. Scalmani, M. J. Frisch, B. Mennucci, J. Tomasi, R. Cammi, V. Barone, *J. Chem. Phys.* **2006**, 124, 94107.
- [82] Y. Tawada, T. Tsuneda, S. Yanagisawa, T. Yanai, K. Hirao, *J. Chem. Phys.* **2004**, 120, 8425–8433.
- [83] M. Caricato, B. Mennucci, J. Tomasi, F. Ingrosso, R. Cammi, S. Corni, G. Scalmani, *J. Chem. Phys.* **2006**, 124, 124520.
- [84] N. M. O’Boyle, A. L. Tenderholt, K. M. Langner, *J. Comput. Chem.* **2008**, 29, 839–845.
- [85] L. Barnes, B. Schindler, A.-R. Allouche, D. Simon, S. Chambert, J. Oomens, I. Compagnon, *Phys. Chem. Chem. Phys.* **2015**, 17, 25705–25713.

Manuscript received: May 30, 2022

Revised manuscript received: August 30, 2022

Accepted manuscript online: September 2, 2022

Version of record online: September 29, 2022